Structural Chemistry and Magnetic Properties of the $BaMn_{0.4}Co_{0.6}O_{2.83}$ Hexagonal Perovskite

L. Miranda, J. Ramírez-Castellanos, A. Varela, J. González-Calbet, and M. Parras*

Departamento de Química Inorgánica, Facultad de Químicas, Universidad Complutense, E-28040 Madrid, Spain

María Hernando and M. T. Fernández-Díaz

Institut Laue Langevin, BP 156X, F-38042 Grenoble, France

M. García Hernández

Instituto de Ciencia de Materiales de Madrid, CSIC, Cantoblanco, E-28049 Madrid Spain

Received November 23, 2006. Revised Manuscript Received January 11, 2007

The complete structural characterization of the hexagonal cobaltite $BaMn_{0.4}Co_{0.6}O_{2.83}$ has been performed by combining high-resolution transmission electron microscopy and electron and neutron diffraction. The structure is closely related to the 12H $(cc'chhh)_2$ with oxygen deficient cubic c′-BaO_2 layers. This framework forms a laminar structure in which tetramers of face-sharing octahedra occupied by manganese and cobalt are connected by corners to two tetrahedral layers mostly occupied by cobalt. A magnetic study shows only the presence of short-range magnetic interactions indicating that there are no interactions between the tetramers through the tetrahedral layers, thus impeding the three-dimensional magnetic ordering of the system. A spin-glass-like state was found to be compatible with the observed phenomenology.

Introduction

The crystal structures of perovskites, ABO_3, can be considered as formed by pseudo-close-packed AO_3 layers, with B cations occupying the oxygen octahedral holes. Depending on the layers stacking, different structures result. If all AO_3 layers stack cubic closed packed (ABC sequence), the $[BO_6]$ octahedra form the three-dimensional (3D) corner-sharing array of the well-known cubic perovskite. This structure is stable for a structural tolerance factor t close to 1 (where $t = d_{A-O}/\sqrt{2}d_{B-O}$). The ideal hexagonal ABO_3 perovskite, the 2H structural type, differs from the cubic perovskite in which all the AO_3 layers are in hexagonal close packing (AB sequence), leading to a hexagonal array of infinite chains of face-sharing $[BO_6]$ octahedra. This one-dimensional structure is adopted by ABO_3 phases containing large A cations. A wide range of hexagonal polytypes have been described between both hexagonal and cubic perovskites, whose structures arise from different periodic cubic (c) and hexagonal (h) mixed sequences of the AO_3 layers.

The cation size, the electronic configuration of the B cations, and the oxygen stoichiometry are factors that strongly influence the stabilization of a particular polytype for a given composition. $BaMnO_3$[1] and $BaCoO_3$[2] crystallize in the 2H hexagonal type (...hhh... sequence). In both systems, the anionic vacancies are accommodated by the introduction of deficient BaO_{3-y} layers leading to the stabilization of different hexagonal polytypes.

$BaCoO_{3-y}$ accommodates the anionic deficiency by the incorporation of BaO_2 cubic layers, giving rise to the formation of tetrahedral sites connected via their vertices to the octahedral ones. A 12H $(cc'chhh)_2$ polytype has been reported for $BaCoO_{2.60}$[3] and, more recently, for barium defective $Ba_{0.9}CoO_{2.60}$[4] oxide, while a 5H (cc′chh) has been stabilized for $BaCoO_{2.80}$.[5] In all of them, the oxygen deficiency is accommodated by c′-BaO_2 layers leading to the formation of oxygen tetrahedra occupied by Co(IV).

On the other hand, a large number of $BaMnO_{3-y}$ ordered phases has been stabilized as a function of the oxygen content: four rhombohedral (33R, 27R, 21R, and 15R) and four hexagonal (8H, 6H, 10H, and 4H) polytypes.[6−9] On the basis of the X-ray and electron diffraction data and high-resolution electron microscopy (HREM) we have suggested that the oxygen deficiency is accommodated in the $BaMnO_{3-y}$ system, by the introduction of cubic $BaO_{2.5}$ layers giving rise to the formation of pyramidal square sites occupied by Mn^{3+}. However, this structural model has been recently contradicted by a neutron diffraction study of the 4H-$BaMnO_{2.65}$ and 4H-$Ba_{0.5}Sr_{0.5}MnO_{2.79}$.[10] The most striking

* Corresponding author. E-mail: mparras@quim.ucm.es. Fax: (34) 91 394 43 52.

(1) Hardy, A. *Acta Crystallogr.* **1962**, *15*, 179.
(2) Taguchi, H.; Takeda, Y.; Kanamaru, F.; Shimada, M.; Koizumi, M. *Acta. Crystallogr.* **1977**, *B33*, 1298.
(3) Jacobson, A. J.; Hutchinson, J. L. *J. Solid State Chem.* **1980**, *35*, 334.
(4) Maignan, A.; Hèrbert, S.; Pelloquin, D.; Pralong, V. *J. Solid State Chem.* **2006**, *179*, 1852.
(5) Boulahya, K.; Parras, M.; González-Calbet, J. M.; Amador, U.; Martínez, J. L.; Tissen, V.; Fernández-Díaz, M. T. *Phys. Rev. B* **2005**, *71*, 144402.
(6) Negas, T.; Roth, R. S. *J. Solid State Chem.* **1971**, *3*, 323.
(7) Parras, M.; González-Calbet, J. M.; Alonso, J.; Vallet-Regí, M. *J. Solid State Chem.* **1994**, *113*, 78.
(8) González-Calbet, J. M.; Parras, M.; Alonso, J.; Vallet-Regí, M. *J. Solid State Chem.* **1994**, *111*, 202.
(9) Parras, M.; Alonso, J.; González-Calbet, J. M.; Vallet-Regí, M. *J. Solid State Chem.* **1995**, *117*, 21.

10.1021/cm062798c CCC: $37.00
Published on Web 02/15/2007

feature of the refined structures for both compounds is the localization of the anion vacancies, predominantly in the face-shared sites to form BaO_{3-y} hexagonal layers.

According to that, although stoichiometric $BaMnO_3$ and $BaCoO_3$ are isostructural, the oxygen deficiency is accommodated in a different way and, consequently, $BaMnO_{3-y}$ and $BaCoO_{3-y}$ stabilize different polytypes with different structural features. Therefore, $BaMn_{1-x}Co_xO_{3-y}$ compounds, with both Mn and Co in the B cationic substructure, can adopt many different stacking sequences of layers of different anionic compositions. In this sense, some data are available for the Ba−Mn−Co−O system. Taguchi et al. have studied the phase formation in stoichiometric $BaMn_{1-x}Co_xO_3$ prepared under high oxygen pressure.[11] The 2H structural type is retained within the compositional range of $0 \leq x \leq 1$. A more complex situation is found when the anionic substructure is not complete and different hexagonal polytypes seem to be stable in this system. Gibb[12] has reported the existence of the 12H and 5H hexagonal polytypes from XRD data for $BaMn_{0.5}Co_{0.5}O_{2.87}$ and $BaMn_{0.2}Co_{0.8}O_{2.80}$, respectively. Besides, the extended X-ray fine structure (EXAFS) study of Co and Mn cations suggests the presence of Co in a tetrahedral oxygen environment indicating the presence of oxygen deficient BaO_2 layers. On the other hand, Cherepanov et al.[13] report the phase equilibrium diagram in the $LaCoO_3$−$LaMnO_3$−$BaMnO_3$ system studied at 1373 K also by powder X-ray diffractometry. According to these results, two structures occur for $BaMn_{1-x}Co_xO_{3-y}$ corresponding to the 10H and 12H hexagonal polytypes, although in this case, only the unit cell parameters are reported. In spite of this, none of the above-mentioned compounds have been structurally characterized, and their physical properties have not been investigated yet.

The magnetic and electrical properties of perovskite oxide are determined by the structures they adopt and, in view of the large interest in the magnetoresistance of Mn oxides, we have undertaken the study of the compounds $BaMn_{1-x}Co_xO_{3-y}$. This paper describes the synthesis, the structural study carried out by using X-ray and neutron diffraction and selected area electron diffraction (SAED), and the magnetic behavior of the 12H-$BaMn_{0.4}Co_{0.6}O_{2.83}$.

Experimental Section

The black polycrystalline sample of $BaMn_{0.4}Co_{0.6}O_{3-y}$ was prepared from a well ground stoichiometric mixture of $BaCO_3$ (Aldrich, 99.98%), $MnCO_3$ (Aldrich, 99%), and Co_3O_4 (Aldrich, 99.98%). The mixture was heated in a platinum crucible at 1223 K in air for 24 h. After, the sample was treated at 1373 K for 2 days and then quenched under liquid nitrogen to room temperature. This process was repeated four times with intermediate grinding to ensure homogeneity.

The average cationic composition was determined by inductively coupled plasma (ICP) whereas the local composition was analyzed by energy-dispersive X-ray spectroscopy (EDS) with an INCA analyzer system attached to a JEOL 3000 FEG electron microscope.

The oxygen content was determined by thermogravimetric analysis (TGA) on a Cahn D-200 electrobalance which allowed for the determination of variations of the oxygen content within $\pm 1 \times 10^{-3}$ on a sample of about 100 mg.

Powder X-ray diffraction (XRD) patterns were collected using Cu Kα_1 monochromatic radiation ($\lambda = 1.540\,56$ Å) at room temperature on a Panalytical X'PERT PRO MPD diffractometer equipped with a germanium(111) primary beam monochromator and X'Celerator fast detector. Neutron powder diffraction (NPD) data were collected at room temperature and at 5 K on the high-resolution powder diffractometer D2B at the Institute Laue Langevin (ILL), Grenoble (France), with neutrons of wavelength 1.594 Å. The angular range covered by the detector expands from 0° to 160° in scattering angle (step size 0.05°). Diffraction data were analyzed by the Rietveld method[14] using the Fullprof program.[15]

SAED and HREM were performed in a JEOL 3000 FEG electron microscope, fitted with a double tilting goniometer stage (±22°, ±22°). Simulated HREM images were calculated by the multislice method using the MacTempas software package.

The magnetization was measured by a commercial superconducting quantum interference device (SQUID) magnetometer from Quantum Design. Transport and magnetotransport measurements were performed by the conventional four-probe technique, under magnetic fields up to 90 kOe in a PPMS system from Quantum Design for a sintered pellet. Previously, the specific heat of the pellet was also measured in the PPMS system at zero magnetic field.

Results and Discussion

The cationic composition, determined on several dozens of small crystallites by EDX analysis in the electron microscope, is in agreement with the nominal one. The oxygen content was determined by TGA by reduction under 200 mbar H_2/300 mbar He atmosphere and heating at 279 K/min up to 1123 K. BaO, MnO, and Co metal was identified by XRD as the final products of the reduction process. The observed weight loss, corresponding to 9.5% of the starting material, leads to the $BaMn_{0.4}Co_{0.6}O_{2.83}$ composition.

The XRD pattern can be indexed on the basis of a hexagonal unit cell with lattice parameters $a = 5.7001(1)$ and $c = 28.6032(2)$ Å, no impurity phases being detected. This unit cell is the expected for a 12H polytype in agreement with previous results. Actually, a 12H-$BaMn_{0.5}Co_{0.5}O_{2.87}$ has been characterized by means of EXAFS.[12] These data were compatible with the $(ccchhh)_2$ layer sequence and support the possible presence of BaO_2 layers and tetrahedral cobalt sites. To confirm these structural features, SAED and HREM were performed.

Parts a, b, and c of Figure 1 show the SAED patterns corresponding to $BaMn_{0.4}Co_{0.6}O_{2.83}$ along [010], [$\bar{1}$10], and [001], respectively. All reflections can be indexed on the basis of a 12H polytype of hexagonal symmetry. The reflection spots observed in the SAED pattern along [$\bar{1}$10] are compatible with space group $P6_3/mmc$ although all of them are visible in the SAED pattern along the [010] zone axis (Figure 1a). Actually, in this pattern the (00l) spots with $l = 2n + 1$ are visible, although they are systematically weaker than those with $l = 2n$. These spots are absent in

(10) Adkin, J. J. A.; Hayward, M. A. *J. Solid State Chem.* **2006**, *179*, 70.
(11) Taguchi, H.; Shimada, M.; Kanamaru, F.; Koizumi, M.; Takeda, Y. *J. Solid State Chem.* **1976**, *18*, 299.
(12) Gibb, T. C. *J. Mater. Chem.* **1992**, *2* (4), 387.
(13) Cherepanov, V. A.; Filonova, E. A.; Voronin, V. I.; Berger, I. F. *J. Solid State Chem.* **2000**, *153*, 205.
(14) Rietveld, H. M. *J. Appl. Crystallogr.* **1969**, *2*, 65.
(15) Rodríguez-Carvajal, J. *Physica B* **1993**, *192*, 55.

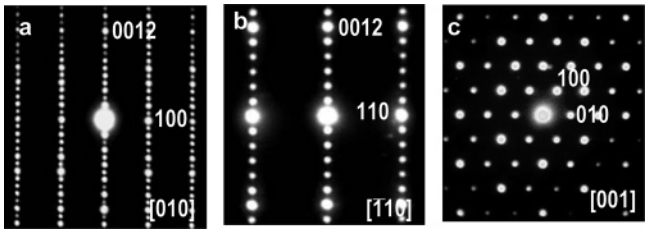

Figure 1. SAED patterns corresponding to $BaMn_{0.4}Co_{0.6}O_{2.83}$ along (a) [010], (b) [$\bar{1}$10], and (c) [001].

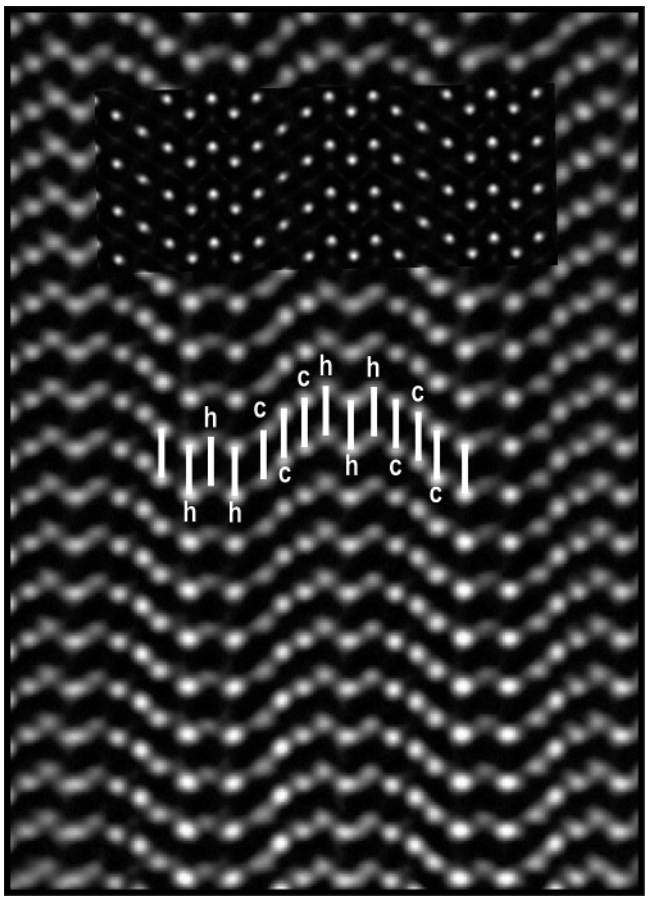

Figure 2. High-resolution transmission electron microscopy image taken along the [010] direction. The calculated image is shown in the inset.

the SAED pattern along [$\bar{1}$10] zone (Figure 1b). This shows that the diffraction conditions are such that the (00l) and (*h*0l) reflections are only present for $l = 2n$; therefore, in the [010] zone the (00l) reflections with $l = 2n + 1$ must be attributed to double diffraction. Figure 2 corresponds to the most relevant HREM image taken along the [010] direction. In this zone, the structure is viewed parallel to the columns of close packed Ba−O rows and, thus, the projected image directly reveals the stacking sequence of the polytype. Under the experimental conditions of the image, Ba atoms are projected as the brightest dots. In the observed contrast, for six adjacent bright dots, segments of five aligned dots are associated to two slope changes; the same sequence is imaged in a mirror up to a 12 layer periodicity. This contrast variation corresponds to a $(hhhccc)_2$ layer sequence.

It is noticeable that no sign of disorder is observed by neither SAED nor HREM. The diffraction spots are sharp without any streak along *c**. Besides, the lack of stacking faults in the HREM discards the presence of intergrowth with other polytypes, the *ccchhh* array being extended through the whole crystal. The image calculated with the ideal atomic positions corresponding to this 12H layers sequence (inset at Figure 2) nicely fits with the experimental one for $\Delta t = 50$ and $\Delta f = -500$ Å.

Table 1. Final Structural Parameters Resulting from the Refinement of $BaMn_{0.4}Co_{0.6}O_{2.83}$[a]

atom	site	*x*/*a*	*y*/*b*	*z*/*c*	occupancy	B_{iso} (Å^2)
Ba(1)	2a	0	0	0	1	*b*
Ba(2)	4f	1/3	2/3	−0.0959(2)	1	1.07(10)
Ba(3)	4f	1/3	2/3	0.1751(2)	1	1.39(12)
Ba(4)	2d	1/3	2/3	3/4	1	1.11(15)
M(1)	4f	1/3	2/3	0.0566(2)	0.930(2)Co/ 0.070(2)Mn	0.22(14)
M(2)	4e	0	0	0.1204(5)	0.510(2)Co/ 0.490(2)Mn	0.95(11)
M(3)	4e	0	0	0.2073(7)	0.294(3)Co/ 0.706(3)Mn	0.45(12)
O(1)	4f	1/3	2/3	−0.0029(3)	1	*c*
O(2)	12k	0.157(1)	2×	0.0820(1)	1	1.25(5)
O(3)	12k	0.151(1)	2×	0.6654(1)	1	1.27(7)
O(4)	6h	0.150(1)	2×	1/4	1	1.01(5)

[a] Space group, $P6_3/mmc$; $a = 5.69348(4)$ Å, $c = 28.5751(3)$ Å. [b,c] Anisotropic temperature factors for (a) Ba(1), $\beta_{11} = 0.0518(2)$, $\beta_{22} = 0.0518(2)$, $\beta_{33} = 0.0004(2)$, $\beta_{12} = 0.0259(4)$, $\beta_{13} = 0$, $\beta_{23} = 0$; (b) O(1), $\beta_{11} = 0.0591(3)$, $\beta_{22} = 0.0591(3)$, $\beta_{33} = 0.0012(1)$, $\beta_{12} = 0.0295(3)$, $\beta_{13} = 0$, $\beta_{23} = 0$. $R_B = 6.04$, $R_{exp} = 4.73$, $R_{wp} = 5.63$, $\chi^2 = 1.42$.

According to these observations, $BaMn_{0.4}Co_{0.6}O_{2.83}$ exhibits a closely related 12H structure, where blocks of four face-sharing octahedra are linked by sharing corners to blocks of two corner-sharing octahedra. In order to perform a detailed structural characterization of the sample, a structural refinement of the NPD data was carried out taking as starting model the ideal atomic positions corresponding to the above-described model in the $P6_3/mmc$ space group. Initially, Mn and cobalt were randomly distributed over the three available crystallographic positions (see Table 1) in a 40/60 ratio according to the $BaMn_{0.4}Co_{0.6}O_{2.83}$ formula. During the early stages of the refinement the absence of O(1) from the 6g site became clear. This fact suggests that the oxygen vacancies are located in the cubic layers of the blocks of the two corner-sharing octahedra. The change of the O(1) from the 6g to the 4f atomic position greatly improves the refinement and leads to a noticeable decreasing of the fit parameters, for instance χ^2 is reduced from 8.1 to 1.4. This change gives rise to tetrahedral coordination for metals located at the M(1) site (4f position), in agreement with the oxygen content obtained by TGA analysis. The same anionic arrangement has been observed in other Co hexagonal polytypes as 12H-$Ba_{0.9}CoO_{2.6}$[4] or 5H-$BaCoO_{2.80}$.[5] In both cases, the presence of cubic BaO_2 layers results in the replacement of the two corner-sharing octahedra by two unconnected tetrahedra stabilizing layered structures in which blocks formed by a limited number of face-sharing octahedra are connected through their terminal corners to two CoO_4 tetrahedra. In 12H-$BaMn_{0.4}Co_{0.6}O_{2.83}$, this ordered anionic vacancy distribution leads to one-third of the metal atoms (M(1)) in oxygen tetrahedral coordination.

Subsequent refinement showed that these M(1) sites are occupied almost by cobalt (∼93%); the octahedral M(2) was found to be occupied by both Co and Mn in equal amounts (∼50%), while the M(3) sites, corresponding to the central positions of the octahedral tetramer, are mainly occupied by

Table 2. Selected Interatomic Distances (Å) in $BaMn_{0.4}Co_{0.6}O_{2.83}$

Ba(1)−O(1)	3.2882(3) ×6	M(1)−O(1)	1.70(1)
Ba(1)−O(2)	2.811(5) ×6	M(1)−O(2)	1.881(8) ×3
Ba(2)−O(1)	2.65(1)	M(2)−O(2)	1.90(1) ×3
Ba(2)−O(2)	2.876(8) ×6	M(2)−O(3)	1.96(1) ×3
Ba(2)−O(3)	2.687(6) ×3		
		M(3)−O(3)	1.90(1) ×3
Ba(3)−O(2)	3.174(5) ×3	M(3)−O(4)	1.92(2) ×3
Ba(3)−O(3)	2.865(5) ×6		
Ba(3)−O(4)	2.800(5) ×3		
		M(2)−M(1)	3.80(3)
Ba(4)−O(4)	2.85(1) ×6	M(2)−M(3)	2.48(2)
Ba(4)−O(3)	3.017(5) ×6	M(3)−M(3)	2.43(3)

Mn (70%) reflecting the strong preference of Mn for face-sharing octahedra sites. This feature has been also observed in other manganese contained hexagonal polytypes, for instance in 6H-$BaMn_{0.767}Fe_{0.233}O_{2.87}$ oxide,[16] 12R-$BaMn_{0.5}Ti_{0.5}O_3$,[17] or 9R-$BaMn_{1-x}Ir_xO_3$.[18] The refined composition $BaMn_{0.42(2)}Co_{0.58(2)}O_{2.83}$ was consistent with the nominal one.

Moreover, from crystallochemical considerations, the tetrahedral positions are most likely occupied by Co^{4+} whereas Co^{3+} is preferably located at the octahedral sites. From this consideration and in accordance with the cationic distribution obtained from this refinement, the following formulation should be proposed: $Ba(Co^{IV}_{0.31}Mn_{0.02})_{td}(Co^{III}_{0.10}Mn_{0.24})_{Oh}(Co^{III}_{0.17}Mn_{0.16})_{Oh}O_{2.83}$. Therefore, the formal oxidation state for the cobalt is close to +3.5 and Co^{4+} and Co^{+3} are present in 54% and 46%, respectively. Finally, manganese, according to the anionic stoichiometry, is almost totally as Mn^{4+} (∼95%).

The refinement was stable, and an isotropic displacement parameter for each atom was refined successfully. The presence of anionic vacancies generates cubic BaO_{3-y} layers that are no longer close-packed, making the atomic displacement through the layer easier. For this reason we have considered an anisotropic displacement parameter for Ba(1) and O(1); the obtained values reflect a large delocalization on the *xy* plane. The refined atomic positions, occupancies, and displacement parameters for 12H-$BaMn_{0.42}Co_{0.58}O_{2.83}$ resulting from the refinement are listed in Table 1, whereas Table 2 collects some selected interatomic distances. Figure 3 shows the graphic result of the fitting of the NPD pattern and the difference between observed and calculated data. A schematic representation of the structure and the polyhedral sites are depicted in Figure 4a,b, respectively. The structure is based on a 12H close packed $(ccchhh)_2$ stacking where one of every three cubic layers presents a BaO_2 anionic composition. It can be described as formed by units of four face-sharing octahedra connected by corner-sharing tetrahedra.

The $M(3)O_6$ octahedron is almost regular with six very close distances with an average $d(M(3)-O) = 1.91$ Å in excellent agreement with Mn−O distances observed for Mn in the same environment, 2H-$BaMnO_3$ (1.9044 Å),[19] 6H-$BaMn_{0.767}Fe_{0.233}O_{2.87}$ (1.92 Å),[16] or 12R-$BaMn_{0.5}Ti0_{.5}O_3$ (1.905 Å).[17] In contrast, the $M(2)O_6$ octahedron is quite distorted with three long and three short M−O distances (see Table 2) indicating that metals in this position are displaced from the center toward the oxygen atoms in the cubic layer (O(2)), that is, to the neighbor tetrahedra sharing corner, and hence away from the shared face. As a consequence, the M(3)−M(3) distance, between cations located in central octahedra, becomes comparable to the M(3)−M(2) distance, corresponding to cations situated in the outer octahedra, thus reducing the electrostatic repulsion between cations in adjacent face-sharing polyhedra. The only nonshared terminal oxygen is O(1) and, as in 5H-$Ba_5Co_5O_{14}$,[5] this Co-terminal oxygen distance is the shortest one in the structure. This short M(1)−O(1) distance is compensated by a large M(1)−O(2) distance giving quite distorted $M(1)O_4$ tetrahedra.

The short distance M(1)−O(1) and the large distance Ba(1)−O(1) arising from the tetrahedral coordination of M(1)

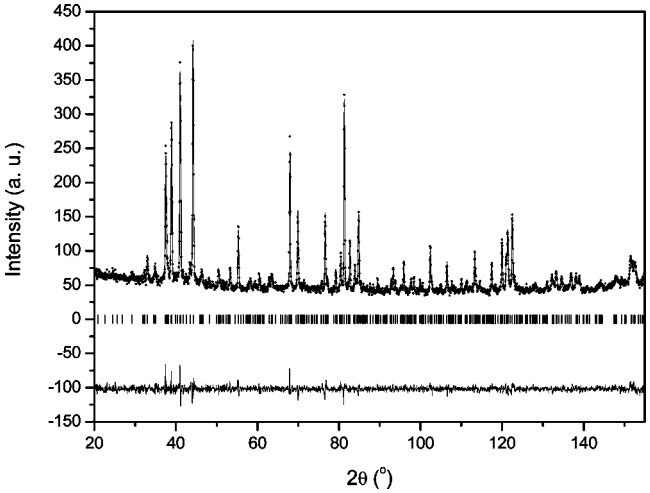

Figure 3. Experimental, calculated, and difference neutron diffraction pattern corresponding to $BaMn_{0.4}Co_{0.6}O_{2.83}$.

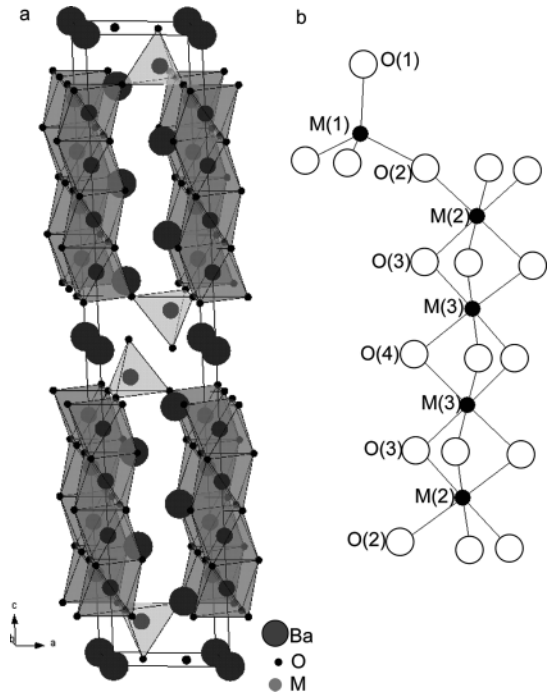

Figure 4. Schematic representation of the structure (a) and the polyhedra sites (b) corresponding to $BaMn_{0.4}Co_{0.6}O_{2.83}$.

(16) Caignaert, V.; Hervieu, M.; Domengès, B.; Nguyen, N.; Pannetier, J.; Raveau, B. *J. Solid State Chem.* **1988**, *73*, 107.
(17) Keith, G. M.; Kirk, C. A.; Sarma, K.; Alford, N. M.; Cussen, E. J.; Rosseinsky, M. J.; Sinclair, D. C. *Chem. Mater.* **2004**, *16*, 2007.
(18) Jordan, N. A.; Battle, P. D. *J. Mater. Chem.* **2003**, *9*, 2220.
(19) Cussen, E. J.; Battle, P. D. *Chem. Mater.* **2000**, *12*, 831.

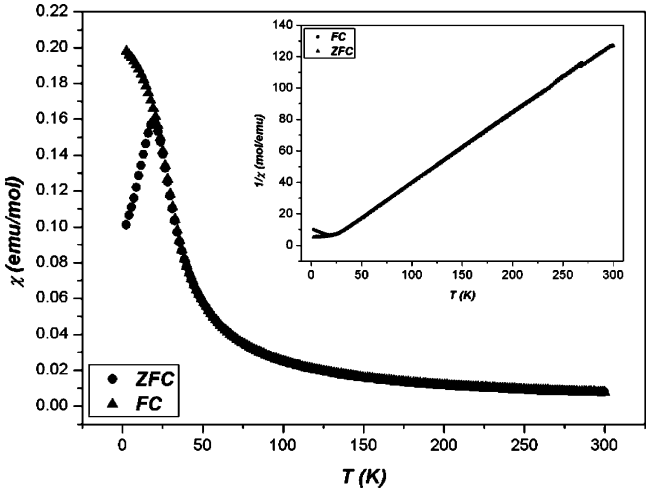

Figure 5. Temperature dependence of the magnetic susceptibility measured at 1 kOe. The inverse of the magnetic susceptibility is shown in the inset.

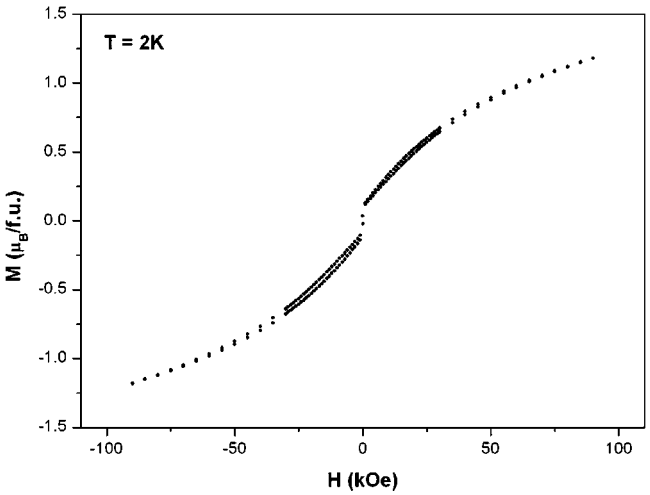

Figure 6. Magnetization curves versus applied magnetic field at different temperatures corresponding to $BaMn_{0.4}Co_{0.6}O_{2.83}$.

leads to a large anisotropy of the displacement parameter for Ba(1) and O(1) in the *xy* plane. As we have mentioned above, the M(1) sites are almost fully occupied by Co, stable in a tetrahedral oxygen environment. On the contrary, Mn is not stable in this coordination, and depending on the oxidation state, it shows preference for either octahedral (Mn^{4+}) or square pyramidal coordination (Mn^{3+}). Therefore, the presence of Mn in this cationic position, even in a small ratio, must induce disorder in the BaO_2 cubic layers which is reflected in the displacement factors. Similar results were obtained by Shpanchenko et al.[20] for $Ba_5Er_2Al_2ZrO_{13}$ and by Gómez et al. for 10H-$BaFeO_{2.80}$;[21] in all these cases the presence of significant anionic disorder gives rise to anomalous displacement parameters.

Various physical properties have been also explored. Figure 5 shows the temperature dependence of the magnetic susceptibility as measured in a field of 1 kOe. As it can be readily seen a clear irreversibility between a zero field cooling (ZFC) and a field cooling (FC) opens up below 20 K. The inverse of the magnetic susceptibility of $BaMn_{0.4}Co_{0.6}O_{2.83}$ (inset in Figure 5) follows a Curie−Weiss law almost in the whole explored range.

The best fit renders an effective paramagnetic moment of 4.3 μ_B/formula unit and a Weiss constant Θ around 11 K. The expected effective moment was calculated (4.8 μ_B/formula unit) from the crystallochemical assumption above-described: Co^{3+} and Co^{4+} located in an octahedral and tetrahedral environment, respectively, and Mn almost totally as Mn^{4+} except a small proportion of Mn^{3+} sited in M(1) sites. Besides, a high spin electronic configuration for Co^{4+} (5.9 μ_B) and Co^{3+} (4.9 μ_B) was considered taking into account those found in Ba_2CoO_4 (Co^{4+} in tetrahedral oxygen environment),[22] and for Co^{3+} it was considered taking into account those in the octahedral site, 5H-$Ba_5Co_5O_{14}$[5] and 12H-$BaCoO_{2.6}$.[3] As it can be observed, the expected effective moment value agrees rather well with calculated one from the slope of the inverse of the magnetic susceptibility. The positive Weiss constant value is indicative of the ferromagnetic character of the magnetic correlations in origin as confirmed by the hysteretic behavior of the isothermal magnetization in Figure 6. The hysteresis loop at low temperature (2 K) exhibits a wasp-waisted shape, characteristic of systems that, although disordered, present some degree of directional ordering that could be translated.[23] Along this line, it should be also noticed that saturation is not reached even at 50 kOe which can be explained in terms of the existence of an important fustration in the system, due probably to the presence of antiferromagnetic correlations. Indeed no long-range 3D order is achieved according to neutron diffraction data. Actually, the neutron diffraction data collected at low temperatures (5 K) can be interpreted using the same crystallographic model, and no additional reflections that could be of magnetic origin were observed. This behavior could point toward the existence of a spin-glass or a spin-glass-like system at low temperatures, as the conditions for magnetic fustration and disorder seem to be present in $BaMn_{0.4}Co_{0.6}O_{2.83}$. Similar hysteresis loops and absence of 3D order were observed for the related compound $Sr_4Mn_2CoO_9$.[24] In this case, it was proposed that the atomic force microscopy correlations would dominate the short-ranged interactions between Mn^{4+} ions in the octahedral sites, but no 3D ordering could be achieved because of the freezing of the interchain interactions at low temperature, where a disordered magnetic state builds up.

To explore the existence of a spin-glass or spin-glass-like state, we have measured the alternating current (AC) susceptibility over a wide range of frequencies (33 Hz, 10 000 Hz), as shown in Figure 7. From the real part of the magnetic susceptibility χ', the shift toward lower temperatures is apparent when the frequency decreases and the calculated $\Delta T_f/(T_f\Delta(\log \omega))$ is around 0.06, as expected for a canonical spin glass.[25] Notice also the agreement between

(20) Shpanchenko, R. V.; Abakumov, A.; Antipov, E. V. *J. Solid State Chem.* **1995**, *118*, 180.
(21) Gómez, M. I.; Lucotti, G.; de Moran, J. A.; Aymonino, P. J.; Pagola, S.; Stephens, P.; Carbonio, R. E. *J. Solid State Chem.* **2001**, *160*, 17.
(22) Jin, R.; Sha, H.; Khalifah, P. G.; Sykora, R. E.; Sales, B. C.; Mandrus, D.; Zhang, J. *Phys. Rev. B* **2006**, *73*, 174404.
(23) *Introduction to Magnetic Materials*; Cullity, D., Ed.; Addison-Wesley: Reading, MA, 1972; pp 362−367.
(24) Boulahya, K.; Parras, M.; González-Calbet, J. M.; Martínez, J. L. *Chem. Mater.* **2005**, *15* (18), 3537.
(25) *Spin glasses: an experimental introduction*; Mydosh, J. A., Ed.; Taylor & Francis: London, 1993; p 66.

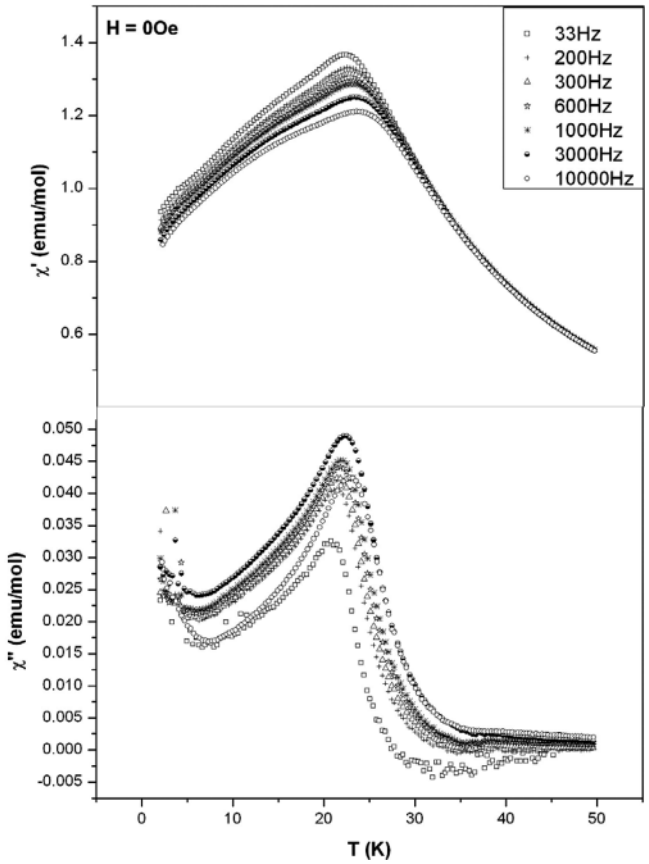

Figure 7. Temperature dependence of the real (χ') and the imaginary parts (χ'') of the AC magnetic susceptibility at different frequencies from 33 to 10 000 Hz.

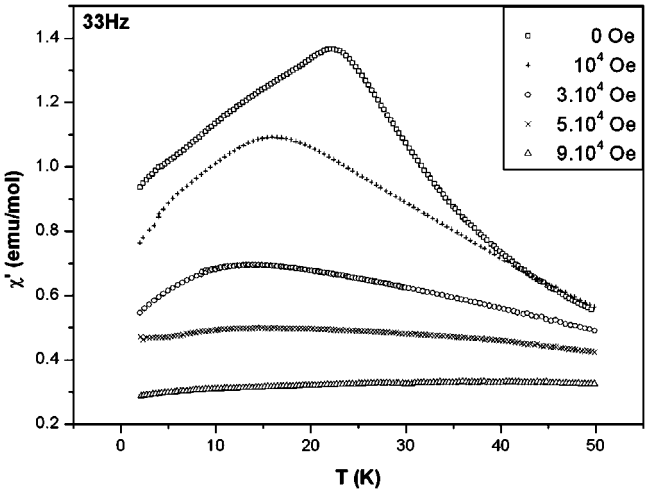

Figure 8. Temperature dependence of the real part of the AC magnetic susceptibility at different applied fields.

the temperatures of the maximum in the imaginary component of the AC magnetic susceptibility, χ'', and that of the cusp signaling the onset of the irreversible behavior in the direct current (DC) magnetization. We have also measured the effect of an applied magnetic field in the AC magnetization. As it is evidenced in Figure 8, the real part of the magnetic susceptiblity flattens as the applied field increases while the peak shifts toward lower temperatures. This magnetic field smearing of the AC magnetization points out that the applied magnetic field strongly suppresses the freezing of the glassy state.

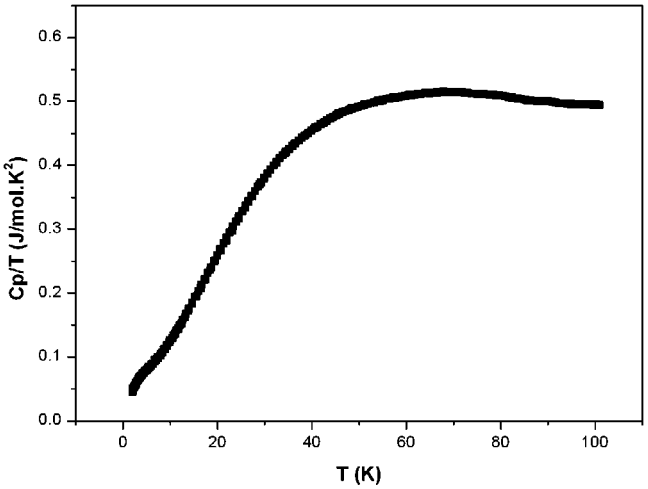

Figure 9. Temperature dependence of the C_p/T measured at zero magnetic field for $BaMn_{0.4}Co_{0.6}O_{2.83}$.

We have measured the resistivity of this material and found an insulating behavior. Indeed, the very high value of the resistivity bellow 200 K does not allow accomplishing the electrical measurements in the low-temperature region. This situation does not improve with the application of an external magnetic field as high as 90 kOe. Therefore, it can be concluded that no evidence of magnetoresistive behavior can be reported, in line with what is observed for isostructural $Ba_{0.9}CoO_{2.6}$.[4]

As shown in Figure 9, the temperature dependence of the measured specific heat, C_p/T, does not exhibit any sharp feature in the temperature range where the magnetic transitions are spotted in the magnetic measurements. The general behavior very much resembles what has been observed in the related compound $Sr_4Mn_2CoO_9$[24] for which a spin-glass-like state was also postulated at low temperatures. With the system being an insulator, only two mayor contributions to the specific heat are expected: lattice (phonons) and magnetic. As seen in Figure 9, the measured specific heat differs from what it is expected from a pure Debye model ($C_p/T \propto T^2$) for which only lattice contributions exist. This difference can be abscribed to a magnetic contribution compatible with the development of a glassy state at temperatures well bellow 100 K in agreement with magnetic and neutron scattering experiments.

From the above-described structural, magnetic, and thermal properties of $BaMn_{0.4}Co_{0.6}O_{2.83}$, it can be concluded that the system conforms to what is expected from a spin-glass system: a large irreversibility in the ZFC−FC DC magnetization, a clear shift of the maximum of the AC magnetic susceptibility with frequency and applied magnetic field, and a clear deviation from a Debye model for the specific heat that can be explained in terms of a large and sharpless magnetic contribution to C_p.

Acknowledgment. Financial support through research Project Nos. MAT2004-01248, CAMS-0505/PPQ/0316, and MAT2005-06024-C02-01 is acknowledged.

CM062798C